

ThermRad: A Multi-modal Dataset for Robust 3D Object Detection under Challenging Conditions

Qiao Yan*, Yihan Wang*
Nanyang Technological University
50 Nanyang Avenue, Singapore
{QIAO003, WANG1517}@e.ntu.edu.sg *

Abstract

Robust 3D object detection in extreme weather and illumination conditions is a challenging task. While radars and thermal cameras are known for their resilience to these conditions, few studies have been conducted on radar-thermal fusion due to the lack of corresponding datasets. To address this gap, we first present a new multi-modal dataset called *ThermRad*, which includes a 3D LiDAR, a 4D radar, an RGB camera and a thermal camera. This dataset is unique because it includes data from all four sensors in extreme weather conditions, providing a valuable resource for future research in this area. To validate the robustness of 4D radars and thermal cameras for 3D object detection in challenging weather conditions, we propose a new multi-modal fusion method called *RTDF-RCNN*, which leverages the complementary strengths of 4D radars and thermal cameras to boost object detection performance. To further prove the effectiveness of our proposed framework, we re-implement state-of-the-art (SOTA) 3D detectors on our dataset as benchmarks for evaluation. Our method achieves significant enhancements in detecting cars, pedestrians, and cyclists, with improvements of over 7.98%, 24.27%, and 27.15%, respectively, while achieving comparable results to LiDAR-based approaches. Our contributions in both the *ThermRad* dataset and the new multi-modal fusion method provide a new approach to robust 3D object detection in adverse weather and illumination conditions. The *ThermRad* dataset will be released.

1. Introduction

Autonomous vehicles rely on a combination of complementary sensors, including cameras, LiDARs, and radars, to achieve robust and precise perception for both 2D and 3D object detection and tracking, as well as semantic and instance segmentation [43,62]. However, although RGB cam-

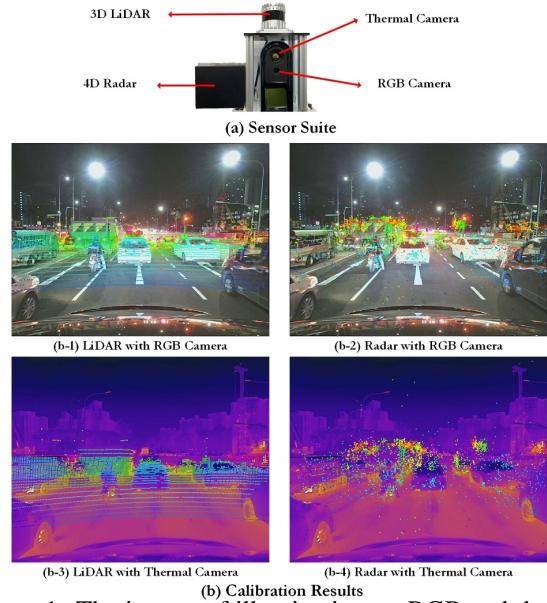


Figure 1: The impact of illumination on RGB and thermal images. While the RGB image is affected by poor lighting conditions, the thermal image remains unaffected. However, the thermal image exhibits blurry object edges.

eras deliver precise edge and color data and LiDARs provide accurate 3D positional information under fair conditions, their performance can be significantly hindered under extreme weather conditions. For example, high and low-intensity illumination can negatively impact the visibility of RGB cameras [29,36], and LiDARs are impeded by their inability to penetrate heavy rain, fog, and snowflakes [38,61]. On the contrary, thermal cameras can capture the infrared radiation emitted by objects, and radars can generate millimeter waves to detect objects, making them more resilient in challenging conditions when RGB cameras and LiDARs fail [20,26,31]. However, a significant challenge remains in addressing the low spatial resolution of 4D radar point clouds and the ambiguous object edges in thermal images [25,30]. As a result, the design of robust perception mod-

** Co-first authorship and corresponding author

Table 1: Comparison of radar datasets.

Dataset	Size	Radar	LiDAR	Camera	Annotations	Extreme Weather	Illumination
Astyx [43]	Small	4D	✓	RGB	3D	✗	Sufficient
RobotCar [3]	Large	3D	✓	RGB	✗	✗	Sufficient, weak
SeeThroughFog [6]	Large	3D	✓	RGB, Thermal	3D	Fog, rain, snow	Sufficient, weak
nuScenes [7]	Large	3D	✓	RGB	3D	Rain	Sufficient, weak
MulRan [32]	Middle	3D	✓	RGB	✗	✗	Sufficient
Zendar [46]	Middle	3D	✓	RGB	2D	✗	Sufficient
CARRADA [49]	Large	3D	✗	RGB	2D	✗	Sufficient
RadarScenes [57]	Large	3D	✗	RGB	2D	✗	Sufficient
RADIATE [58]	Large	3D	✓	RGB	2D	Fog, rain, snow	Sufficient, weak
RADDET [75]	Large	3D	✗	RGB	3D	✗	Sufficient
K-Radar [50]	Large	4D	✓	RGB	3D	Fog, rain, snow	Sufficient, weak
VoD [51]	Large	4D	✓	RGB	3D	✗	Sufficient
RADIAL [53]	Middle	4D	✓	RGB	2D	✗	Sufficient
TJ4DRadSet [76]	Middle	4D	✓	RGB	3D	✗	Sufficient, weak
ThermRad (Ours)	Middle	4D	✓	RGB, Thermal	3D	Rain	Sufficient, weak

ules necessitates a meticulous integration of these modalities to overcome their inherent limitations.

3D object detection has been revolutionized by deep learning, which relies on large annotated datasets for training neural networks to recognize multi-class objects [2, 76]. However, popular datasets such as the KITTI [21] and the Waymo Open Dataset [62] lack both radar and thermal data, thus presenting limitations when dealing with adverse weather conditions. Similarly, the nuScenes [7] does not include thermal images and only provides 3D radar data without elevation information. The absence of multi-modal data limits the development of robust perception systems. Although the emergence of 4D radars capturing range, azimuth, Doppler and elevation, has led to the creation of several multi-modal datasets [43, 50, 51, 76], these studies indicate sub-optimal performances of radar-based methods, especially in detecting small objects like pedestrians and cyclists. To enhance the precision of radar-based methods, the integration of complementary sensors is often required [6, 28, 48]. Particularly in severe weather conditions, commonly-used LiDARs and RGB cameras prove ineffective, making thermal cameras the only viable option [5]. Despite their potential for robust object detection in challenging environments, there is currently no research on the fusion of 4D radars and thermal cameras. Therefore, to bridge this research gap, we present a novel multi-modal dataset, ThermRad, together with a novel framework, *RTDF-RCNN*, tailored for this dataset. ThermRad is the first to include a 4D radar, a thermal camera, a 3D LiDAR, and an RGB camera under challenging weather conditions. *RTDF-RCNN* enables the deep fusion of data from thermal cameras and 4D radars for robust 3D object detection.

1.1. Contribution

Our contributions can be summarized as follows:

(a) We introduce a unique dataset, ThermRad, designed for robust 3D object detection in adverse weather conditions. To the best of our knowledge, it is the first dataset incorporating a 4D radar and a thermal camera with a 3D LiDAR and an RGB camera as auxiliary modalities.

(b) We provide the dataset with comprehensive coverage of weather, lighting, and road conditions, including challenging scenarios such as poor illumination at night, as well as light and heavy rainfall. These intentionally included cases enable the evaluation of robust 3D object detection under adverse weather conditions, where the performance of RGB and LiDAR modalities are affected while the thermal camera and radar remain less impacted.

(c) We establish a benchmark by evaluating existing state-of-the-art detectors on both radar and LiDAR modalities, serving as baselines for future research facilitation and performance comparison.

(d) We introduce *RTDF-RCNN*, pioneering work deeply fusing 4D radar point clouds and thermal images for robust 3D object detection. Through extensive experiments, we demonstrate the significant superiority of *RTDF-RCNN* over existing 3D detectors under challenging weathers.

(e) We propose two modules to identify and address the domain gap between different modalities. Primarily, the domain gap between RGB and thermal cameras is tackled by introducing a lightweight, end-to-end trainable 2D backbone. Secondly, the Geometric-aware Cross-Attention (GaCA) module is proposed to bridge the domain gap between 4D radar and thermal modalities.

2. Related Works

2.1. Radar Dataset

The availability of various modalities of datasets plays a crucial role in advancing autonomous driving techniques. However, there are limited datasets that include radars, despite their cost-efficiency and capability in challenging weather conditions. For robust 3D detection, it is crucial to consider the following factors when using multi-modal data: (a) the utilization of Doppler, range, azimuth, and elevation information with the emergence of 4D radars; (b) the integration of information from complementary modalities; (c) the inclusion of severe weather conditions to maximize data diversity.

As summarized in Table 1, several datasets have been developed using 3D radars without elevation data, such as RobotCar [3] and MulRan [32], which utilize a scanning 3D radar and a LiDAR for place recognition and odometry construction. RADDet [75] collects 3D radar data at urban roadways and proposes dynamic object recognition on spectrum images to anticipate items from a bird’s-eye view (BEV). Similarly, RadarScenes [57] offers 3D radar points and RGB images with 2D boxes as ground truth from city traffic, while CARRADA [49] collects range-azimuth-Doppler images under a simulated environment with a maximum of two objects per frame. SeeThrough-Fog [6], nuScenes [7], and RADIATE [58] datasets thoughtfully account for a variety of weather situations.

Recently, a few benchmarks with 4D radar data have been released [43, 50, 51, 53, 76]. However, Astyx [43] is limited by its size of 500 frames, and RADIAL [53] only supports *Cars* object detection. TJ4DRadSet [76] and VoD [51] are published and evaluated by exploring classes of uniformly allocated objects. The large-scale K-Radar [50] benchmark is the first to explore the impact of diverse weather conditions on object detection performance. Although its inclusion of LiDAR and RGB images, K-Radar heavily relies on 4D radar under adverse weather conditions. This dependence on a single modality with sparse point clouds in challenging conditions could restrict the dataset’s applicability.

2.2. Radar and Thermal Detection

Radar Detection. Various methods detect 2D objects using 3D radars. For example, [13, 18, 33] regress 2D bounding boxes under BEV, while [56] clusters objects using semantic features. Some approaches combine the radar with other modalities. [47] introduces a two-stage framework to output anchor boxes, and [48] projects radar points into images to estimate 3D objects by pillar expansion. RadarNet [73] considers the sparsity of radar and the density of LiDAR for feature extraction with an early-fusion strategy. Later, [52] refines RadarNet and integrates re-

gion of interests (RoI) pooling into a fusion module to locate 2D objects. Only a few works are developed based on 4D radars. Meyer et al. [44] adopt a radar-camera detection method similar to [37] and later propose a graph convolutional network to process radar data [45]. RPFANet [70] introduces a feature-attention module to improve results on the Astyx dataset, while CramNet [28] proposes a ray-constrained mechanism to fuse features from radars and RGB cameras. Some studies [43, 51, 76] implement LiDAR-based detectors as a baseline. Additionally, [50] proposes two network structures to improve the performance.

Thermal Detection. Thermal cameras have gained attention for pedestrian detection, surveillance, and autonomous driving due to their advantages in dim conditions compared to vision-based cameras [4, 10]. The KAIST multi-spectral pedestrian benchmark [29] has accelerated the development of thermal-image-based object detection techniques. [1, 22] use Faster R-CNN [54] and report the augmentation effect by salient maps specifically on thermal images. Other methods [10, 35, 40, 66] use fusion networks that add two parallel input streams of color images and thermal images, resulting in multispectral detection.

3. Dataset Details

3.1. Sensor Setup and Data Acquisition

The brief specifications of sensors are listed as follows:

4D radar: Oculii Eagle, 77GHz working frequency, up to 400m range, 0.86m range accuracy and resolution, 45° vertical field-of-view (FoV) with 0.175° accuracy, 113° horizontal FoV with 0.44° accuracy, 12Hz FPS.

3D LiDAR: Ouster OS1-32, 32 channels, 100m range with 80% Lambertian reflectivity and 45m range with 10% Lambertian reflectivity, 3cm range accuracy, 45° vertical FoV with 0.01° accuracy, 360° horizontal FoV with 0.01° accuracy, 10Hz FPS, with internal IMU.

RGB Camera: SY020HD-V1, 3.5mm focal length, 60° vertical FoV, 70° horizontal FoV, 640 × 480 resolution, 30Hz FPS.

Thermal Camera: InfiRay MicroIII, 8μm – 14μm spectral band, 12μm pixel pitch, 5.8mm focal length, 55° vertical FoV, 65° horizontal FoV, 640 × 512 resolution, 25Hz FPS.

As shown in Figure 1, a 4D radar, a thermal camera, a 3D LiDAR, and an RGB camera, are positioned on a fixed platform atop a vehicle. These sensors are collectively calibrated following [17]. Our dataset encompasses a diverse range of weather and illumination conditions. These include fair weather, light and heavy rainfall, along with various lighting scenarios such as normal daylight, intense traffic lights, and ill-illuminated conditions during both day and night. The data collection process involves driving across diverse road types, including urban roads with and without

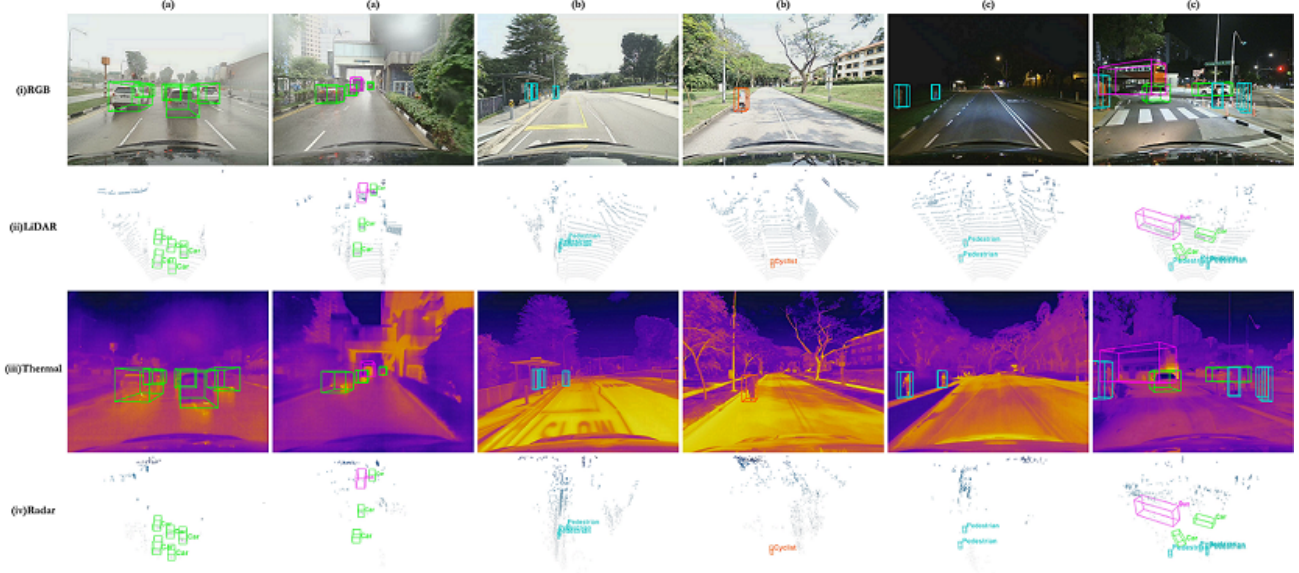


Figure 2: Examples of ground truth annotations. (i) RGB camera, (ii) 3D LiDAR, (iii) thermal camera and (iv) 4D radar are four modalities in our dataset. Different columns show varied weather conditions: (a) rain, (b) daytime, (c) nighttime. Car, pedestrian, cyclist and bus are presented in green, blue, orange, and purple 3D bounding boxes respectively.

traffic, suburban areas, mountain lanes, parking lots, sidewalks, intersections, and construction zones, ensuring comprehensive coverage of road environments.

3.2. Dataset Statistics

We collect a total of approximately 3 hours of data consisting of 48 sequences, each lasting around 2-5 minutes. To ensure data synchronization, we utilize the arrival time of the data as the timestamp and apply filtering techniques described in [51]. We collect a total of 100,000 frames, and to balance the coverage of different scene types, every 50th frame is manually labeled. We exhaustively annotate all appearing objects within the range $[0 < x < 50m, -25m < y < 25m]$ under the LiDAR coordinate and within the common FoV of all sensors, resulting in 4724 ground truth multi-class objects (car, pedestrian, cyclist, and bus). The annotations include the object's 3D locations in x, y, z axis, length (l), width (w), height (h), and rotation angle (θ). These annotations can be transformed into the coordinates of the radar and thermal camera, and they adhere to the same formats and definitions as the KITTI dataset, making them compatible with existing toolkits. We categorize the dataset into two subregions based on the radial distance toward the vehicle: (a) 0-25m and (b) 25m+. Figure 2 illustrates representative scenes captured under different circumstances. For training and evaluation purposes, we select a subset of 2000 frames, dividing them into a 75% training set and a 25% testing set. Importantly, frames from the same sequence are exclusively assigned to one set to avoid any bias. More examples and detailed descriptions are provided in the supplementary material.

To protect human privacy, we artificially put mosaic to human faces to ensure that all RGB images featuring humans do not contain identifiable facial features.

3.3. Evaluation Metrics

We follow [21] and adopt the Average Precision (AP) based on the Intersection over Union (IoU) as evaluation metrics for 3D object detection. We calculate AP on both 3D (AP_{3D}) and BEV (AP_{BEV}) with the IoU threshold at 0.5 for car, 0.25 for pedestrian and 0.25 for cyclist.

4. RTDF-RCNN

We propose a novel 3D object detection framework, *RTDF-RCNN*, utilizing both 4D radar point clouds and thermal images in a deep-fusion approach. It is an end-to-end pipeline consisting of five modules: a 2D backbone, a 3D backbone, a region proposal network (RPN), a box refinement module, and a novel GaCA module. Our proposed *RTDF-RCNN* effectively fuses multi-modal features in multiple stages. The overall architecture is depicted in Figure 3.

In the first stage, the thermal image is fed into the 2D backbone to extract pixel-wise features, while the 4D radar point clouds is voxelized and encoded by the 3D backbone. To leverage information from two modalities, we introduce a novel Geometric-aware Cross-Attention (GaCA) module that combines radar and thermal features with corresponding geometric information to produce a fused feature map. The RPN then embeds the fused feature maps provided by the backbone to generate estimated proposals. In the second stage, RoI pooling is adopted to aggregate sparse vol-

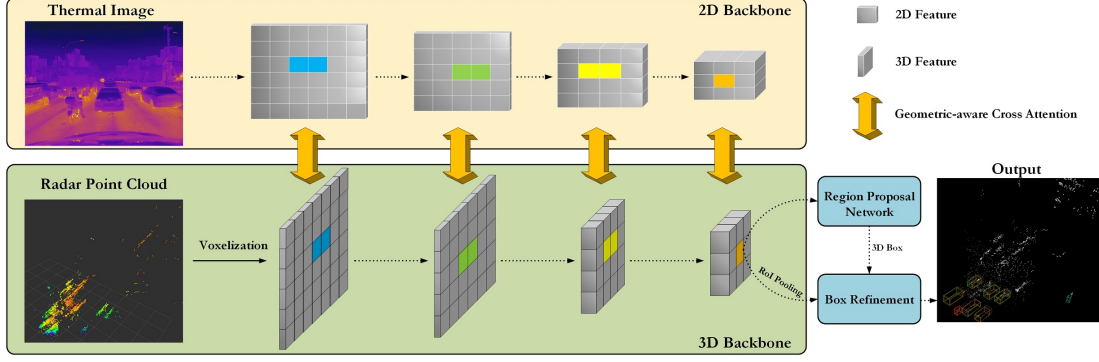


Figure 3: The flowchart of *RTDF-RCNN*. The 4D radar point cloud is voxelized as 3D sparse voxels and processed by our 3D backbone, while the thermal image features are extracted by our 2D backbone. Geometric-aware Cross-Attention modules are embedded to leverage the optimal associations between 3D and 2D representations. Feature maps are encoded by the RPN to generate proposals and features are pooled with the RoI-grid pooling module for refining proposals.

umes comprised of multi-modal features. Eventually, the RoI pooled features are encoded by multilayer perceptrons for accurate box refinement.

4.1. 2D Backbone

CenterFusion [48] is a typical approach for integrating multi-modal inputs, specifically correlating 3D radar point clouds with RGB images. However, its effectiveness heavily depends on the accuracy of existing 2D object detectors such as CenterNet [19]. Besides other similar methods [28, 60, 65, 67] also rely on heavyweight 2D models to generate semantic information. This not only adds computations but also requires additional annotation efforts to bridge the domain gap between RGB and thermal cameras.

To address these issues, our 2D backbone is proposed. Firstly, we overcome the limitations of applying external detectors by directly utilizing thermal images as the native representation of heat maps. Secondly, we employ a lightweight network, BasicBlock [27], to extract heat map features and significantly reduce computational complexity. Additionally, our end-to-end trainable network alleviate the domain gap between RGB and thermal cameras for eliminating the need for extra annotation. The thermal image I_0 with spatial resolution $C \times H \times W = 3 \times 640 \times 512$ is encoded successively by four BasicBlocks with $[1, 2, 4, 8]$ downsampling stride to extract image features I_1, I_2, I_3 and I_4 with spatial size $C_1 \times H \times W, C_2 \times \frac{H}{2} \times \frac{W}{2}, C_3 \times \frac{H}{4} \times \frac{W}{4}$ and $C_4 \times \frac{H}{8} \times \frac{W}{8}$ respectively.

Compared with existing methods [28, 48, 60, 65, 67], our 2D backbone not only addresses the domain gap between RGB and thermal cameras but also overcomes the challenge of computational complexity for effective feature extraction of thermal images.

4.2. 3D Backbone

3D sparse convolution [24] is a popular approach in LiDAR-based detectors [16, 59, 60, 72, 77, 78] for its efficiency and accuracy. The usage of 3D convolutional neural networks (CNNs) as the backbone in radar-based methods has been limited due to the lack of elevation information in 3D radars. With the advent of 4D radars, incorporating elevation information to extract 3D features has become innate, achieved through the integration of 3D CNNs.

The raw radar point clouds are indicated as $X, Y, Z, Power, Doppler$, where X, Y, Z are the coordinates of points and $Power, Doppler$ represent the detected signal-to-noise ratio and Doppler velocity. The sparse radar points P are first uniformly sampled and scattered into 3D voxels V_0 with $L = 5$ channels as input. 3D voxels V_0 are then sequentially embedded by four 3D CNNs to generate V_1, V_2, V_3 and V_4 3D feature volumes with same $[1, 2, 4, 8]$ downsampling stride and $[C_1, C_2, C_3, C_4]$ channels in parallel with the 2D backbone. Specifically, at each stage, the 3D CNN takes the sparse volumes which are a combination of radar voxel features and thermal image features as input described in Eq (1). To facilitate the fusion mechanism, the channel numbers of features from two parallel streams, V_i and I_i , where $i = 1, 2, 3, 4$, remain consistent.

$$\begin{aligned} V_i &= Conv3D(V_{i-1}), I_i = Conv2D(I_{i-1}) \\ V_i &= GaCA(V_i, I_i), \text{ where } i = 1, 2, 3, 4 \end{aligned} \quad (1)$$

The obtained multi-modal features V_4 are fed into the RPN composed of top-down and upsampling modules to encode the feature map to provide high-quality 3D anchors based on methods in [39, 72].

4.3. Radar-Thermal Fusion

[41] identifies the domain gap between two distinct modalities resulting in unsatisfactory feature extraction

performance. Therefore, we propose a Geometric-aware Cross-Attention module in order to better align features and modalities' associations, while maintaining our framework end-to-end trainable. This method is presented as an enhancement over prior techniques, such as CramNet [28] and DeepFusion [41]. In CramNet, a ray-constrained attention module is designed to estimate point coordinates and capitalize on the ambiguity of geometric correlations but it fails to resolve the feature correspondences. Yet, its superiority compels us to concentrate on the effect of geometric positions. Hence, we add the measured 3D positions of 4D radar point clouds into the attention head to better harness the connections between features from two modalities, named geometric awareness. Compared to DeepFusion, our Geometric-aware Cross-Attention module replaces one input stream with 3D spatial information, and it is embedded into the backbone at multiple stages to thoroughly align features from 4D radar point clouds and thermal images.

The 3D feature volumes $\mathbf{V}_i = \{\mathbf{P}_i \in \mathbb{R}^{N \times 3}, \mathbf{F}_i \in \mathbb{R}^{N \times C_i}\}$ where N voxels are associated with their 3D coordinates \mathbf{P}_i and feature vectors \mathbf{F}_i , are firstly projected into image plane. Then N matched image feature pixels \mathbf{I}_i are selected and stacked into a feature vector with identical size $N \times C_i$. As described in Eq (2), features vector \mathbf{F}_i , their 3D coordinates \mathbf{P}_i and selected \mathbf{I}_i are transformed as *query*, *key* and *value*. Then *query*, *key* and *value* are processed by an attention head [64] and a following fully connected layer to aggregate multi-modal features. The aggregated features are concatenated with the original feature vector \mathbf{F}_i . Finally, the output vector \mathbf{F}_i is applied to construct 3D feature volumes $\mathbf{V}_i = \{\mathbf{P}_i \in \mathbb{R}^{N \times 3}, \mathbf{F}_i \in \mathbb{R}^{N \times 2C_i}\}$ where \mathbf{P}_i and \mathbf{P}_i are identical as 3D coordinates. We fuse multi-modal features at four stages $i = 1, 2, 3, 4$ for promoting deep-fusion.

$$\begin{aligned} q &= FC(\mathbf{F}_i), k = FC(\mathbf{P}_i), v = FC(\mathbf{I}_i) \\ \mathbf{F}_i &= Concat(FC(AttentionHead(q, k, v)), \mathbf{F}_i) \end{aligned} \quad (2)$$

A typical issue stated in [9] is that conventional augmentation techniques including flipping, scaling and rotation of point clouds lead to data misalignment. To tackle this issue, we employ the solution in [9, 41] that reversely transforms the augmented point clouds into original coordinates before the fusion operation. We skip the ground-truth sampling augmentation [72], which selects samples from the database and pastes them into point clouds and images since our dataset lacks 2D annotations in the image plane.

By incorporating the relationship between radar and thermal features with corresponding 3D coordinates, each feature point is weighted by its 3D coordinates. Using our attention mechanism, we establish a soft correlation between radar point clouds and thermal images, thereby enabling adaptive fusion.

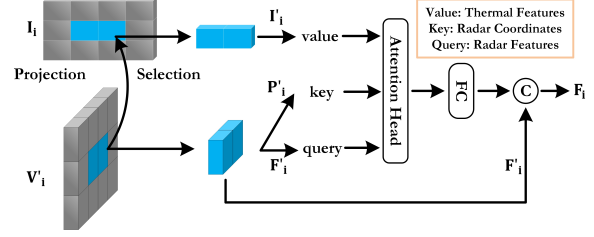


Figure 4: Geometric-aware Cross-Attention module for multi-modal fusion, encoding thermal features, radar features, and coordinates with an attention mechanism.

4.4. Box Refinement and Loss Function

Box Refinement. For each 3D anchor, we sample point-wise features after a division with $10 \times 10 \times 10$ grids within \mathbf{V}_4 as expressed in Eq (3). After that, these representatives are stacked as feature vectors and encoded by two multilayer perceptions (*MLP*) to precisely forecast the displacement and classification of each anchor. To assign each anchor to its corresponding ground truth, we use the IoU-based method with varying thresholds for each class following [39, 59, 72]. The significance of the two-stage detector is the separation of the refinement network from the RPN and the independent branch for finetuning box parameters.

$$\begin{aligned} \mathcal{S} &= \{s_1, s_2, \dots, s_{1000}\}, \text{ where } s_i \in \mathbf{V}_4 \\ \mathcal{LOC} &= MLP_1(\mathcal{S}) \\ \mathcal{CLS} &= MLP_2(\mathcal{S}) \end{aligned} \quad (3)$$

Loss Function. The localization of refined boxes generated by *MLP* and their match ground truth are denoted as $(x_a, y_a, z_a, l_a, w_a, h_a, \theta_a)$ and $(x_g, y_g, z_g, l_g, w_g, h_g, \theta_g)$ and the predicted probability of classification is revealed as p_a . To regress the localization and classification, we apply the SmoothL1 loss function and the focal loss function in an identical approach as [39, 72].

5. Experimental Results

This section comprehensively implements a few SOTA single-modal and multi-modal 3D detectors for quantitative comparison. We primarily address specific details on implementation and then examine their performances.

5.1. Implementing Details

To correspond with the standard settings of each model, we adjust the point cloud range to $[0 < x < 51.6\text{m}, -25.6\text{m} < y < 25.6\text{m}, -2\text{m} < z < 2\text{m}]$, and reset the pillar size at $[x=0.16\text{m}, y=0.16\text{m}, z=4\text{m}]$ with 32 and 16 maximum number of points per pillar for LiDAR and radar, voxel size at $[x=0.05\text{m}, y=0.05\text{m}, z=0.1\text{m}]$ with a maximum of 5 points per voxel for both LiDAR and radar. We specify the anchor box sizes for *car*, *pedestrian* and *cyclist* as $[4.24\text{m}, 1.99\text{m},$

Table 2: Performance on LiDAR and RGB camera. “L” means LiDAR-only and “L+R” means LiDAR-RGB fusion.

Method	Modal	Car				Pedestrian				Cyclist			
		$AP_{3D}(\%)$		$AP_{BEV}(\%)$		$AP_{3D}(\%)$		$AP_{BEV}(\%)$		$AP_{3D}(\%)$		$AP_{BEV}(\%)$	
		0-25m	25m+	0-25m	25m+	0-25m	25m+	0-25m	25m+	0-25m	25m+	0-25m	25m+
SECOND [72]	L	90.85	77.92	90.85	78.64	86.64	66.68	86.87	66.68	89.52	71.35	89.62	71.35
PointPillars [39]	L	90.69	70.59	90.73	75.71	83.97	51.96	84.22	52.66	78.13	65.58	78.18	65.58
PV-RCNN [59]	L	94.61	79.22	94.69	79.92	86.27	76.06	86.30	76.11	89.71	73.49	89.73	73.49
Voxel R-CNN [16]	L	90.42	68.37	90.48	70.66	85.66	50.34	85.95	50.74	80.54	63.99	80.74	64.05
EQ-PVRCNN [74]	L	90.43	71.39	90.56	74.84	84.52	57.18	84.52	57.18	72.19	41.86	72.19	41.86
PointPainting+PointPillars [65]	L+R	68.27	52.75	75.72	56.95	66.76	30.91	67.12	30.91	65.04	45.04	67.75	47.80
PV-RCNN+Focals Conv [9]	L+R	94.82	81.12	94.85	82.12	79.23	70.11	79.32	70.16	89.82	70.59	90.42	70.59
Voxel R-CNN+Focals Conv [9]	L+R	90.67	72.83	90.71	75.11	77.44	50.05	77.44	50.05	81.21	60.83	81.21	60.83
PV-RCNN+3D-DF [34]	L+R	94.42	80.12	94.81	80.24	75.66	70.12	76.30	70.12	88.54	70.11	88.67	70.11
Voxel R-CNN+3D-DF [34]	L+R	90.72	69.74	90.78	72.06	80.46	49.65	80.86	49.65	80.43	63.52	89.43	63.52
DeepFusion [41]	L+R	93.42	80.32	93.56	81.25	86.84	73.69	87.10	73.72	86.92	72.54	87.24	72.65

Table 3: Performance on radar and thermal camera. “R” means radar-only and “R+T” means radar-thermal fusion.

Method	Modal	Car				Pedestrian				Cyclist			
		$AP_{3D}(\%)$		$AP_{BEV}(\%)$		$AP_{3D}(\%)$		$AP_{BEV}(\%)$		$AP_{3D}(\%)$		$AP_{BEV}(\%)$	
		0-25m	25m+	0-25m	25m+	0-25m	25m+	0-25m	25m+	0-25m	25m+	0-25m	25m+
SECOND [72]	R	67.97	34.31	76.14	44.83	38.39	20.36	38.27	20.36	37.85	19.02	37.85	19.67
PointPillars [39]	R	71.50	44.23	75.47	50.34	25.74	15.76	27.51	15.76	39.49	21.48	44.07	22.61
PV-RCNN [59]	R	<u>75.64</u>	45.05	<u>78.39</u>	51.21	26.22	15.12	29.59	15.12	33.29	12.63	33.46	12.63
Voxel R-CNN [16]	R	50.39	21.70	51.08	21.82	24.09	14.05	27.09	14.75	25.95	18.09	25.98	18.09
EQ-PVRCNN [74]	R	71.35	40.34	71.54	40.34	25.74	14.25	27.51	15.23	30.43	12.10	31.31	12.10
RPFA-Net [70]	R	72.24	46.52	75.62	50.68	26.67	18.91	28.73	19.12	38.12	21.10	39.64	21.65
RTNH [50]	R	71.03	45.24	71.20	45.62	35.24	20.32	36.10	20.54	38.12	19.54	38.86	20.10
PointPainting+PointPillars [65]	R+T	53.58	35.14	55.44	37.48	30.43	19.70	32.69	19.41	38.87	19.60	43.46	20.01
PV-RCNN+Focals Conv [9]	R+T	70.12	44.49	71.35	44.49	24.12	14.56	25.36	14.82	30.12	10.52	21.56	10.68
Voxel R-CNN+Focals Conv [9]	R+T	48.52	20.79	50.82	20.35	20.21	15.12	20.31	15.12	21.12	12.34	21.12	12.34
PV-RCNN+3D-DF [34]	R+T	75.12	<u>46.32</u>	76.86	<u>52.30</u>	29.86	20.32	30.12	20.32	36.87	14.59	37.12	14.59
Voxel R-CNN+3D-DF [34]	R+T	50.18	31.31	50.46	31.33	24.11	19.82	24.21	19.82	30.52	18.94	30.52	18.94
CenterFusion [48]	R+T	65.24	38.23	65.48	38.62	24.56	17.52	24.68	17.52	38.83	19.54	39.10	19.86
DeepFusion [41]	R+T	70.45	45.64	70.48	45.82	38.42	20.64	38.48	20.68	37.84	20.10	37.86	20.18
RTDF-RCNN(ours)	R+T	83.62	79.51	84.06	79.70	62.66	52.50	69.97	52.50	66.64	44.49	66.69	44.49
Improvements(%)		7.98	33.19	5.67	27.40	24.24	31.86	31.49	31.82	27.15	23.01	22.62	21.88

1.76m], [0.68m, 0.68m, 1.69m] and [1.79m, 0.79m, 1.63m] with the format of [length, width, height] based on our annotations. *RTDF-RCNN* is trained by Adam optimizer with 0.003 learning rate for 100 epochs. All models are trained and tested on 4 RTX 2080Ti GPUs and codes are built on OpenPCDet toolbox [63]. More detailed settings are in the supplementary materials.

5.2. LiDAR and Radar Results

We train SOTA 3D detectors on our dataset as baselines for future works’ references. Particularly, all multi-modal detectors (Focals Conv [9], PointPainting [65], 3D-DF [34], CenterFusion [48] and DeepFusion [41]) use pre-trained 2D model such as DeepLabv3+ [8], CenterNet [19] and U-net [55], as the 2D feature extractor.

Table 2 illustrates the detection results of LiDAR-based and LiDAR-RGB fusion methods. The results indicate that the ‘L+R’ fusion does not yield an improvement in overall performance (*e.g.* the second row and the sixth row, the third row and the seventh row, *etc.*). In some cases, the addition even leads to a worse performance compared to the original LiDAR-only pipeline. This suggests that the addi-

tion of RGB data is not beneficial in our extreme weather scenarios since the RGB camera is significantly affected.

To ensure a fair comparison, we exclude radar-based detectors designed for 2D object detection using 3D radar data [12–15, 18, 47, 69, 73, 75], as they are not suitable for our dataset that includes 4D radar for 3D object detection. Instead, we implement a selected set of radar-based methods, including [48, 50, 70], specifically tailored for 3D object detection on our dataset. Interestingly as stated in Table 3, we observe a decrease in performance when applying the DeepLabv3+ model in PointPainting and Focals Conv to thermal images (*e.g.* the second row and the eighth row, the third row and the ninth row, the fourth row and the tenth row, *etc.*). Since thermal cameras are resilient to extreme weather while DeepLabv3+ struggles to extract features from thermal image representations, this suggests a domain gap between RGB and thermal modalities. Figure 5 directly provides evidence supporting our assertion of a domain gap between RGB and thermal cameras and highlights the challenges associated with feature extraction by applying a pre-trained DeepLabV3+ model on both RGB and thermal images. 3D-DF addresses this issue by using

attention modules to leverage cross-modality features, resulting in a slight improvement in performance.

RTDF-RCNN outperforms all other detectors by its superior feature fusion mechanism and achieves competitive results to LiDAR-based methods. Additionally, we underline the second-best results among all methods to display the improvements. For *cars* within 25m, *RTDF-RCNN* increases AP_{3D} and AP_{BEV} by 7.98% and 5.69% respectively. At distances greater than 25m, other algorithms have trouble identifying objects whereas *RTDF-RCNN* still achieves good results by boosting AP_{3D} by 33.19% and AP_{BEV} by 27.04%. Especially, *RTDF-RCNN* displays tremendous advantages in recognizing *pedestrians* and *cyclists* at all ranges. For example within 25m, *RTDF-RCNN* lifts AP_{3D} and AP_{BEV} by 24.24% and 31.86% for *pedestrians* while by 27.15% and 23.01% for *cyclists*. These boosts benefit from the robustness of thermal camera for generating heat maps and our design of *RTDF-RCNN*.

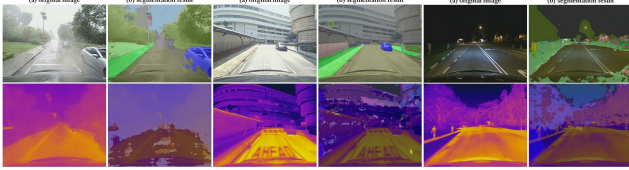


Figure 5: Segmentation results of implementing a pre-trained DeepLabV3+ provided by [11] on RGB and thermal images.

5.3. Ablation Studies

We conduct extensive experiments to validate the effectiveness of the radar-thermal fusion module in our proposed *RTDF-RCNN*. (i) *Fusion methods*. We compare the Geometric-aware Cross-Attention module (GaCA) with summation (Sum.), concatenation (Con.), and LearnableAlign (L.A.), a cross-attention module in DeepFusion. Table 4 indicates the performance of GaCA and L.A. cross-attention over two other methods, validating that simply feature concatenation or summation cannot comprehend the complementary data from 4D radar and thermal camera. Notably, GaCA dramatically exceeds L.A. by novelty preserving 3D geometric information. (ii) *Fusion stages*. Table 5 reveals that GaCA plays a crucial role in the multi-stage fusion process, as the performance of our method is significantly improved with the increase of fusion stages.

Table 4: Performance of different fusion methods.

Method	<i>Car</i> $AP_{3D}(\%)$		<i>Ped.</i> $AP_{3D}(\%)$		<i>Cyc.</i> $AP_{3D}(\%)$	
	0-25m	25m+	0-25m	25m+	0-25m	25m+
GaCA	83.62	79.51	62.66	52.50	66.64	44.49
L.A.	69.12	46.33	43.54	34.85	44.28	20.85
Con.	60.23	39.31	41.18	34.22	22.33	20.96
Sum.	60.48	40.82	37.01	34.65	16.88	9.09

We further analyze the model complexity in Table 6.

The last row reveals that the performance of the proposed *RTDF-RCNN* surpasses other multi-modal-based frameworks in both model parameters and inference speed.

Table 5: Performance at different fusion stages.

Number of Fusion Stage				<i>Car</i> $AP_{3D}(\%)$	
$i = 1$	$i = 2$	$i = 3$	$i = 4$	0-25m	25m+
			✓	78.12	71.35
		✓	✓	80.74	73.49
	✓	✓	✓	81.05	76.54
✓	✓	✓	✓	83.62	79.51

Additionally, we evaluate the effectiveness of the selected 4D radar and the thermal camera for dealing with adverse weather conditions by implementing a combination of different input modalities into our framework as elaborated in Table 7. The improvement of (3) over (1) and (4) over (2) demonstrates the superiority of 4D radar over LiDAR under challenging rain conditions, whereas the enhancement of (4) over (3) and (2) over (1) validates the robustness of thermal camera over RGB camera.

Table 6: Comparison of model parameters and FPS.

Method	Modal	Params. (10^6)	FPS (H_z)
PointPillars+PointPainting [65]	R+T	67.38	3.7
PV-RCNN+Focals Conv [9]	R+T	53.00	24.15
Voxel R-CNN+Focals Conv [9]	R+T	47.49	29.33
PV-RCNN+3D-DF [9]	R+T	52.76	16.09
Voxel R-CNN+3D-DF [9]	R+T	47.24	26.38
<i>RTDF-RCNN</i> (ours)	R+T	19.03	38.31

Table 7: *Car* $AP_{3D}(\%)$ evaluation on separate conditions.

Method:Modality	Day		Night		Rain	
	0-25m	25m+	0-25m	25m+	0-25m	25m+
PointPillars:LiDAR	94.67	84.42	94.72	71.89	78.82	66.36
(1)ours:LiDAR+RGB	94.82	82.45	94.23	79.45	78.25	65.53
(2)ours:LiDAR+Thermal	92.42	83.10	95.05	81.25	79.56	70.38
(3)ours:Radar+RGB	88.24	81.76	84.25	75.24	80.84	70.65
(4)ours:Radar+Thermal	85.31	82.03	84.61	79.92	81.72	77.72

6. Conclusion

This paper introduces ThermRad, the first multi-modal dataset comprising data collected by a 4D radar, a thermal camera, a 3D LiDAR, and an RGB camera under adverse weather and lighting conditions. We annotate and analyze four object categories for robust 3D object detection. To validate the robustness of 4D radars and thermal cameras for 3D object detection in challenging weather, we propose *RTDF-RCNN*, a two-stage pioneering framework specifically designed for thermal images and 4D radar point clouds. We address the domain gap between RGB and thermal cameras by our 2D backbone and bridge the domain gap between 4D radar and thermal cameras by our proposed GaCA. We conduct extensive experimental analysis and demonstrate that *RTDF-RCNN* outperforms state-of-the-art

radar-based methods by a significant margin and achieves comparable performance to LiDAR. Our study contributes a new multi-modal dataset with varying conditions and highlights the effectiveness of 4D radars and thermal cameras for robust 3D object detection under challenging weathers.

References

- [1] Fatih Altay and Senem Velipasalar. The use of thermal cameras for pedestrian detection. *IEEE Sensors Journal*, 22(12):11489–11498, 2022.
- [2] Eduardo Arnold, Omar Y. Al-Jarrah, Mehrdad Dianati, Saber Fallah, David Oxtoby, and Alex Mouzakitis. A survey on 3d object detection methods for autonomous driving applications. *IEEE Transactions on Intelligent Transportation Systems*, 20(10):3782–3795, 2019.
- [3] Dan Barnes, Matthew Gadd, Paul Murcutt, Paul Newman, and Ingmar Posner. The oxford radar robotcar dataset: A radar extension to the oxford robotcar dataset. In *2020 IEEE International Conference on Robotics and Automation (ICRA)*, pages 6433–6438. IEEE, 2020.
- [4] Djamila Romaiissa Beddiar, Brahim Nini, Mohammad Sabokrou, and Abdenour Hadid. Vision-based human activity recognition: a survey. *Multimedia Tools and Applications*, 79:30509–30555, 2020.
- [5] Abhay Singh Bhadoriya, Vamsi Vegamoor, and Sivakumar Rathinam. Vehicle detection and tracking using thermal cameras in adverse visibility conditions. *Sensors*, 22(12), 2022.
- [6] Mario Bijelic, Tobias Gruber, Fahim Mannan, Florian Kraus, Werner Ritter, Klaus Dietmayer, and Felix Heide. Seeing through fog without seeing fog: Deep multimodal sensor fusion in unseen adverse weather. In *Proceedings of the IEEE/CVF Conference on Computer Vision and Pattern Recognition*, pages 11682–11692, 2020.
- [7] Holger Caesar, Varun Bankiti, Alex H Lang, Sourabh Vora, Venice Erin Liong, Qiang Xu, Anush Krishnan, Yu Pan, Giancarlo Baldan, and Oscar Beijbom. nuscenes: A multi-modal dataset for autonomous driving. In *Proceedings of the IEEE/CVF conference on computer vision and pattern recognition*, pages 11621–11631, 2020.
- [8] Liang-Chieh Chen, Yukun Zhu, George Papandreou, Florian Schroff, and Hartwig Adam. Encoder-decoder with atrous separable convolution for semantic image segmentation. In *Proceedings of the European conference on computer vision (ECCV)*, pages 801–818, 2018.
- [9] Yukang Chen, Yanwei Li, Xiangyu Zhang, Jian Sun, and Jiaya Jia. Focal sparse convolutional networks for 3d object detection. In *Proceedings of the IEEE/CVF Conference on Computer Vision and Pattern Recognition*, pages 5428–5437, 2022.
- [10] Hangil Choi, Seungryong Kim, Kihong Park, and Kwanghoon Sohn. Multi-spectral pedestrian detection based on accumulated object proposal with fully convolutional networks. In *2016 23rd International Conference on Pattern Recognition (ICPR)*, pages 621–626. IEEE, 2016.
- [11] MMSegmentation Contributors. MMSegmentation: Openmmlab semantic segmentation toolbox and benchmark. <https://github.com/open-mmlab/mms Segmentation>, 2020.
- [12] Yahia Dalbah, Jean Lahoud, and Hisham Cholakkal. Radar-former: Lightweight and accurate real-time radar object detection model. In *Scandinavian Conference on Image Analysis*, pages 341–358. Springer, 2023.
- [13] Andreas Danzer, Thomas Griebel, Martin Bach, and Klaus Dietmayer. 2d car detection in radar data with pointnets. In *2019 IEEE Intelligent Transportation Systems Conference (ITSC)*, pages 61–66. IEEE, 2019.
- [14] Colin Decourt, Rufin van Rullen, Didier Salle, and Thomas Oberlin. A recurrent cnn for online object detection on raw radar frames. *ArXiv*, abs/2212.11172, 2022.
- [15] Colin Decourt, Rufin VanRullen, Didier Salle, and Thomas Oberlin. Darod: A deep automotive radar object detector on range-doppler maps. In *2022 IEEE Intelligent Vehicles Symposium (IV)*, pages 112–118, 2022.
- [16] Jiajun Deng, Shaoshuai Shi, Peiwei Li, Wengang Zhou, Yanyong Zhang, and Houqiang Li. Voxel r-cnn: Towards high performance voxel-based 3d object detection. In *Proceedings of the AAAI Conference on Artificial Intelligence*, volume 35, pages 1201–1209, 2021.
- [17] Joris Domhof, Julian F. P. Kooij, and Darius M. Gavrilă. A joint extrinsic calibration tool for radar, camera and lidar. *IEEE Transactions on Intelligent Vehicles*, 6(3):571–582, 2021.
- [18] Maria Dreher, Emeç Erçelik, Timo Bänziger, and Alois Knol. Radar-based 2d car detection using deep neural networks. In *2020 IEEE 23rd International Conference on Intelligent Transportation Systems (ITSC)*, pages 1–8. IEEE, 2020.
- [19] Kaiwen Duan, Song Bai, Lingxi Xie, Honggang Qi, Qingming Huang, and Qi Tian. Centernet: Keypoint triplets for object detection. In *Proceedings of the IEEE/CVF international conference on computer vision*, pages 6569–6578, 2019.
- [20] Rikke Gade and Thomas B Moeslund. Thermal cameras and applications: a survey. *Machine vision and applications*, 25(1):245–262, 2014.
- [21] Andreas Geiger, Philip Lenz, Christoph Stiller, and Raquel Urtasun. Vision meets robotics: The kitti dataset. *International Journal of Robotics Research (IJRR)*, 2013.
- [22] Debasmita Ghose, Shasvat M Desai, Sneha Bhattacharya, Deep Chakraborty, Madalina Fiterau, and Tauhidur Rahman. Pedestrian detection in thermal images using saliency maps. In *Proceedings of the IEEE/CVF Conference on Computer Vision and Pattern Recognition Workshops*, pages 0–0, 2019.
- [23] Debasmita Ghose, Shasvat M Desai, Sneha Bhattacharya, Deep Chakraborty, Madalina Fiterau, and Tauhidur Rahman. Pedestrian detection in thermal images using saliency maps. In *Proceedings of the IEEE/CVF Conference on Computer Vision and Pattern Recognition Workshops*, pages 0–0, 2019.
- [24] Benjamin Graham, Martin Engelcke, and Laurens van der Maaten. 3d semantic segmentation with submanifold sparse convolutional networks. In *Proceedings of the IEEE Conference on Computer Vision and Pattern Recognition (CVPR)*, June 2018.

- [25] Zeyu Han, Jiahao Wang, Zikun Xu, Shuocheng Yang, Lei He, Shaobing Xu, and Jianqiang Wang. 4d millimeter-wave radar in autonomous driving: A survey, 2023.
- [26] Kyle Harlow, Hyesu Jang, Tim D. Barfoot, Ayoung Kim, and C. Heckman. A new wave in robotics: Survey on recent mmwave radar applications in robotics. *ArXiv*, abs/2305.01135, 2023.
- [27] Kaiming He, Xiangyu Zhang, Shaoqing Ren, and Jian Sun. Deep residual learning for image recognition. In *Proceedings of the IEEE conference on computer vision and pattern recognition*, pages 770–778, 2016.
- [28] Jyh-Jing Hwang, Henrik Kretschmar, Joshua Manela, Sean Rafferty, Nicholas Armstrong-Crews, Tiffany Chen, and Dragomir Anguelov. Cramnet: Camera-radar fusion with ray-constrained cross-attention for robust 3d object detection. In *Computer Vision–ECCV 2022: 17th European Conference, Tel Aviv, Israel, October 23–27, 2022, Proceedings, Part XXXVIII*, pages 388–405. Springer, 2022.
- [29] Soonmin Hwang, Jaesik Park, Namil Kim, Yukyung Choi, and In So Kweon. Multispectral pedestrian detection: Benchmark dataset and baseline. In *Proceedings of the IEEE conference on computer vision and pattern recognition*, pages 1037–1045, 2022.
- [30] Hamlyn G. Jones and Xavier R. R. Sirault. Scaling of thermal images at different spatial resolution: The mixed pixel problem. *Agronomy*, 4(3):380–396, 2014.
- [31] Kelsey Judd, Michael Thornton, and Austin Richards. Automotive sensing: assessing the impact of fog on lwir, mwir, swir, visible, and lidar performance. page 50, 05 2019.
- [32] Giseop Kim, Yeong Sang Park, Younghun Cho, Jinyong Jeong, and Ayoung Kim. Mulran: Multimodal range dataset for urban place recognition. In *2020 IEEE International Conference on Robotics and Automation (ICRA)*, pages 6246–6253. IEEE, 2020.
- [33] Sangtae Kim, Seunghwan Lee, Seungho Doo, and Byonghyo Shim. Moving target classification in automotive radar systems using convolutional recurrent neural networks. In *2018 26th European Signal Processing Conference (EUSIPCO)*, pages 1482–1486. IEEE, 2018.
- [34] Yecheol Kim, Konyul Park, Minwook Kim, Dongsuk Kum, and Jun Won Choi. 3d dual-fusion: Dual-domain dual-query camera-lidar fusion for 3d object detection. *arXiv preprint arXiv:2211.13529*, 2022.
- [35] Daniel Konig, Michael Adam, Christian Jarvers, Georg Layer, Heiko Neumann, and Michael Teutsch. Fully convolutional region proposal networks for multispectral person detection. In *Proceedings of the IEEE Conference on Computer Vision and Pattern Recognition Workshops*, pages 49–56, 2017.
- [36] Andrew Kramer and Christoffer Heckman. *Radar-Inertial State Estimation and Obstacle Detection for Micro-Aerial Vehicles in Dense Fog*, pages 3–16. 03 2021.
- [37] Jason Ku, Melissa Mozifian, Jungwook Lee, Ali Harakeh, and Steven L Waslander. Joint 3d proposal generation and object detection from view aggregation. In *2018 IEEE/RSJ International Conference on Intelligent Robots and Systems (IROS)*, pages 1–8. IEEE, 2018.
- [38] Akhil M Kurup and Jeremy P. Bos. Dsor: A scalable statistical filter for removing falling snow from lidar point clouds in severe winter weather. *ArXiv*, abs/2109.07078, 2021.
- [39] Alex H Lang, Sourabh Vora, Holger Caesar, Lubing Zhou, Jiong Yang, and Oscar Beijbom. Pointpillars: Fast encoders for object detection from point clouds. In *Proceedings of the IEEE/CVF conference on computer vision and pattern recognition*, pages 12697–12705, 2019.
- [40] Chengyang Li, Dan Song, Ruofeng Tong, and Min Tang. Illumination-aware faster r-cnn for robust multispectral pedestrian detection. *Pattern Recognition*, 85:161–171, 2019.
- [41] Yingwei Li, Adams Wei Yu, Tianjian Meng, Ben Caine, Jiquan Ngiam, Daiyi Peng, Junyang Shen, Yifeng Lu, Denny Zhou, and Quoc V Le. Deepfusion: Lidar-camera deep fusion for multi-modal 3d object detection. In *Proceedings of the IEEE/CVF Conference on Computer Vision and Pattern Recognition*, pages 17182–17191, 2022.
- [42] Tsung-Yi Lin, Priya Goyal, Ross Girshick, Kaiming He, and Piotr Dollár. Focal loss for dense object detection. In *Proceedings of the IEEE international conference on computer vision*, pages 2980–2988, 2017.
- [43] Michael Meyer and Georg Kuschik. Automotive radar dataset for deep learning based 3d object detection. In *2019 16th European Radar Conference (EuRAD)*, pages 129–132, 2019.
- [44] Michael Meyer and Georg Kuschik. Deep learning based 3d object detection for automotive radar and camera. In *2019 16th European Radar Conference (EuRAD)*, pages 133–136. IEEE, 2019.
- [45] Michael Meyer, Georg Kuschik, and Sven Tomforde. Graph convolutional networks for 3d object detection on radar data. In *Proceedings of the IEEE/CVF International Conference on Computer Vision*, pages 3060–3069, 2021.
- [46] Mohammadreza Mostajabi, Ching Ming Wang, Darsh Ranjan, and Gilbert Hsyu. High-resolution radar dataset for semi-supervised learning of dynamic objects. In *Proceedings of the IEEE/CVF Conference on Computer Vision and Pattern Recognition Workshops*, pages 100–101, 2020.
- [47] Ramin Nabati and Hairong Qi. Rrpn: Radar region proposal network for object detection in autonomous vehicles. In *2019 IEEE International Conference on Image Processing (ICIP)*, pages 3093–3097. IEEE, 2019.
- [48] Ramin Nabati and Hairong Qi. Centerfusion: Center-based radar and camera fusion for 3d object detection. In *Proceedings of the IEEE/CVF Winter Conference on Applications of Computer Vision*, pages 1527–1536, 2021.
- [49] Arthur Ouaknine, Alasdair Newson, Julien Rebut, Florence Tupin, and Patrick Perez. Carrada dataset: Camera and automotive radar with range-angle-doppler annotations. In *2020 25th International Conference on Pattern Recognition (ICPR)*, pages 5068–5075. IEEE, 2020.
- [50] Dong-Hee Paek, Seung-Hyun Kong, and Kevin Tirta Wijaya. K-radar: 4d radar object detection for autonomous driving in various weather conditions. In *Thirty-sixth Conference on Neural Information Processing Systems Datasets and Benchmarks Track*, 2022.

- [51] Andras Palffy, Ewoud Pool, Srimannarayana Baratam, Julian F. P. Kooij, and Darius M. Gavrilu. Multi-class road user detection with 3+1d radar in the view-of-delft dataset. *IEEE Robotics and Automation Letters*, 7(2):4961–4968, 2022.
- [52] Kun Qian, Shilin Zhu, Xinyu Zhang, and Li Erran Li. Robust multimodal vehicle detection in foggy weather using complementary lidar and radar signals. In *Proceedings of the IEEE/CVF Conference on Computer Vision and Pattern Recognition*, pages 444–453, 2021.
- [53] Julien Rebut, Arthur Ouaknine, Waqas Malik, and Patrick Pérez. Raw high-definition radar for multi-task learning. In *Proceedings of the IEEE/CVF Conference on Computer Vision and Pattern Recognition*, pages 17021–17030, 2022.
- [54] Shaoqing Ren, Kaiming He, Ross Girshick, and Jian Sun. Faster r-cnn: Towards real-time object detection with region proposal networks. *Advances in neural information processing systems*, 28, 2015.
- [55] Olaf Ronneberger, Philipp Fischer, and Thomas Brox. U-net: Convolutional networks for biomedical image segmentation. In *Medical Image Computing and Computer-Assisted Intervention–MICCAI 2015: 18th International Conference, Munich, Germany, October 5–9, 2015, Proceedings, Part III*, pages 234–241. Springer, 2015.
- [56] Ole Schumann, Markus Hahn, Jürgen Dickmann, and Christian Wöhler. Semantic segmentation on radar point clouds. In *2018 21st International Conference on Information Fusion (FUSION)*, pages 2179–2186. IEEE, 2018.
- [57] Ole Schumann, Markus Hahn, Nicolas Scheiner, Fabio Weishaupt, Julius F Tilly, Jürgen Dickmann, and Christian Wöhler. Radarscenes: A real-world radar point cloud data set for automotive applications. In *2021 IEEE 24th International Conference on Information Fusion (FUSION)*, pages 1–8. IEEE, 2021.
- [58] Marcel Sheeny, Emanuele De Pellegrin, Saptarshi Mukherjee, Alireza Ahrabian, Sen Wang, and Andrew Wallace. Radiate: A radar dataset for automotive perception in bad weather. In *2021 IEEE International Conference on Robotics and Automation (ICRA)*, pages 1–7. IEEE, 2021.
- [59] Shaoshuai Shi, Chaoxu Guo, Li Jiang, Zhe Wang, Jianping Shi, Xiaogang Wang, and Hongsheng Li. Pv-rcnn: Point-voxel feature set abstraction for 3d object detection. In *Proceedings of the IEEE/CVF Conference on Computer Vision and Pattern Recognition*, pages 10529–10538, 2020.
- [60] Vishwanath A Sindagi, Yin Zhou, and Oncel Tuzel. Mvx-net: Multimodal voxelnet for 3d object detection. In *2019 International Conference on Robotics and Automation (ICRA)*, pages 7276–7282. IEEE, 2019.
- [61] Joseph W. Starr and Brian Y. Lattimer. Evaluation of navigation sensors in fire smoke environments. *Fire Technology*, 50:1459–1481, 2014.
- [62] Pei Sun, Henrik Kretschmar, Xerxes Dotiwalla, Aurelien Chouard, Vijaysai Patnaik, Paul Tsui, James Guo, Yin Zhou, Yuning Chai, Benjamin Caine, et al. Scalability in perception for autonomous driving: Waymo open dataset. In *Proceedings of the IEEE/CVF conference on computer vision and pattern recognition*, pages 2446–2454, 2020.
- [63] OpenPCDet Development Team. Openpcdet: An open-source toolbox for 3d object detection from point clouds. <https://github.com/open-mmlab/OpenPCDet>, 2020.
- [64] Ashish Vaswani, Noam Shazeer, Niki Parmar, Jakob Uszkoreit, Llion Jones, Aidan N Gomez, Łukasz Kaiser, and Illia Polosukhin. Attention is all you need. *Advances in neural information processing systems*, 30, 2017.
- [65] Sourabh Vora, Alex H Lang, Bassam Helou, and Oscar Beijbom. Pointpainting: Sequential fusion for 3d object detection. In *Proceedings of the IEEE/CVF conference on computer vision and pattern recognition*, pages 4604–4612, 2020.
- [66] Jörg Wagner, Volker Fischer, Michael Herman, Sven Behnke, et al. Multispectral pedestrian detection using deep fusion convolutional neural networks. In *ESANN*, volume 587, pages 509–514, 2016.
- [67] Chunwei Wang, Chao Ma, Ming Zhu, and Xiaokang Yang. Pointaugmenting: Cross-modal augmentation for 3d object detection. In *Proceedings of the IEEE/CVF Conference on Computer Vision and Pattern Recognition*, pages 11794–11803, 2021.
- [68] Li Wang, Xinyu Zhang, Jun Li, Baowei Xu, Rong Fu, Haifeng Chen, Lei Yang, Dafeng Jin, and Lijun Zhao. Multi-modal and multi-scale fusion 3d object detection of 4d radar and lidar for autonomous driving. *IEEE Transactions on Vehicular Technology*, 72(5):5628–5641, 2023.
- [69] Yizhou Wang, Zhongyu Jiang, Xiangyu Gao, Jenq-Neng Hwang, Guanbin Xing, and Hui Liu. Rodnet: Radar object detection using cross-modal supervision. In *Proceedings of the IEEE/CVF Winter Conference on Applications of Computer Vision*, pages 504–513.
- [70] Baowei Xu, Xinyu Zhang, Li Wang, Xiaomei Hu, Zhiwei Li, Shuyue Pan, Jun Li, and Yongqiang Deng. Rpf-net: a 4d radar pillar feature attention network for 3d object detection. In *2021 IEEE International Intelligent Transportation Systems Conference (ITSC)*, pages 3061–3066. IEEE, 2021.
- [71] Guohang Yan, Zhuochun Liu, Chengjie Wang, Chunlei Shi, Pengjin Wei, Xinyu Cai, Tao Ma, Zhizheng Liu, Zebin Zhong, Yuqian Liu, et al. Opencalib: A multi-sensor calibration toolbox for autonomous driving. *Software Impacts*, 14:100393, 2022.
- [72] Yan Yan, Yuxing Mao, and Bo Li. Second: Sparsely embedded convolutional detection. *Sensors*, 18(10):3337, 2018.
- [73] Bin Yang, Runsheng Guo, Ming Liang, Sergio Casas, and Raquel Urtasun. Radarnet: Exploiting radar for robust perception of dynamic objects. In *European Conference on Computer Vision*, pages 496–512. Springer, 2018.
- [74] Zetong Yang, Li Jiang, Yanan Sun, Bernt Schiele, and Jia-ya Jia. A unified query-based paradigm for point cloud understanding. In *Proceedings of the IEEE/CVF Conference on Computer Vision and Pattern Recognition*, pages 8541–8551, 2022.
- [75] Ao Zhang, Farzan Erlik Nowruz, and Robert Laganier. Raddet: Range-azimuth-doppler based radar object detection for dynamic road users. In *2021 18th Conference on Robots and Vision (CRV)*, pages 95–102. IEEE, 2021.
- [76] Lianqing Zheng, Zhixiong Ma, Xichan Zhu, Bin Tan, Sen Li, Kai Long, Weiqi Sun, Sihan Chen, Lu Zhang, Mengyue Wan,

Libo Huang, and Jie Bai. Tj4dradset: A 4d radar dataset for autonomous driving. In 2022 IEEE 25th International Conference on Intelligent Transportation Systems (ITSC), pages 493–498, 2022.

- [77] Yin Zhou, Pei Sun, Yu Zhang, Dragomir Anguelov, Jiyang Gao, Tom Ouyang, James Guo, Jiquan Ngiam, and Vijay Vasudevan. End-to-end multi-view fusion for 3d object detection in lidar point clouds. In Conference on Robot Learning, pages 923–932. PMLR, 2019.
- [78] Yin Zhou and Oncel Tuzel. Voxelnet: End-to-end learning for point cloud based 3d object detection. In Proceedings of the IEEE conference on computer vision and pattern recognition, pages 4490–4499, 2018.